applied sciences

MDPI

Article

Numerical Study on the Effect of Non-Sinusoidal Motion on the Energy Extraction Performance of Parallel Foils

Yulu Wang, Fahui Zhu and Yonghui Xie *

Shaanxi Engineering Laboratory of Turbomachinery and Power Equipment, School of Energy and Power Engineering, Xi'an Jiaotong University, Xi'an, Shaanxi Province 710049, China; wangyulu@stu.xjtu.edu.cn (Y.W.); zhufahui@stu.xjtu.edu.cn (F.Z.)

* Correspondence: yhxie@mail.xjtu.edu.cn; Tel.: +86-29-82664443

Received: 2 January 2019; Accepted: 20 January 2019; Published: 23 January 2019

Abstract: The effect of non-sinusoidal motion which influences the energy extraction performance of foil is considered in this paper. Two oscillation motions, the combined non-sinusoidal plunging and sinusoidal pitching motion, as well as the combined non-sinusoidal pitching and sinusoidal plunging motion, are selected to investigate the oscillation process of two-dimensional parallel foils numerically. The optimal oscillation motion and average power coefficient at different combined motions are gained. The effects of the plunging motion and pitching motion at different oscillation motions are analyzed, and the evolution law of the foil lift force and vortex field are obtained. It is indicated that the non-sinusoidal motion has a significant influence on energy extraction. When the motion is combined (non-sinusoidal plunging and sinusoidal pitching motion), the best extraction performance is gained at $K_h = -0.5$. The maximal C_{Pm} is 0.375 and the maximal η is 0.188. When the motion is combined (non-sinusoidal pitching and sinusoidal plunging motion), the maximal C_{Pm} is 0.623 and the maximal η is 0.312 which appear at $K_\theta = 2$. For the same frequency, the more the plunging motion is similar to the sinusoidal motion, the more energy is extracted by foils. While the more the pitching motion approximates to the square wave, the worse the achieved extraction performance is.

Keywords: parallel foils; energy extraction performance; non-sinusoidal motion; evolution of the vortex field

1. Introduction

As a new energy extraction device using clean energy, foil is thought to have a bright prospect, especially in the current situation of energy shortages and environmental pollution. Since the combined plunging and pitching motion was put forward and realized to extract energy in 1981 [1], plenty of researchers have discussed the energy extraction characteristics of foil by numerical and experimental methods. According to the laminar computation model, Campobasso et al. [2] simulated the energy extraction performance of foil at a low-velocity flow field with $Re = 1100$. It was found that the energy extraction efficiency can achieve 35% and the deep stall of airfoil has a positive effect on efficiency. Abiru [3] discussed the energy extraction performance and the effect factors (such as the plunging and pitching amplitude, frequency and the free stream velocity) by experiments. The results showed that the power coefficient and efficiency increase with the increase in the amplitude. The experiment system efficiency is observed to be at least 32%. A wind energy extraction device was designed by Shimizu et al. [4], which is based on the flutter mechanism of foil. The device worked under a low frequency and gained a high extraction performance and efficiency. Bryant et al. [5] established a quasi-stable state model and a semi-empirical model of dynamic stall, optimizing the aerodynamic

force and energy extraction performance of foil. They observed that the semi-empirical model of the dynamic stall is effective in predicting the aerodynamic force and efficiency. The numerical research on the extraction performance of foil discusses the potential effect factors like the oscillation motion, the motion parameter, the *Re* number and the profile of foil by the control variable method and the traditional optimization algorithm, aiming at finding a higher power output and extraction efficiency [6–13]. The oscillation process always adopts the sinusoidal motion, however, some researchers tried to use non-sinusoidal motion on foil for further investigations. Platzer et al. [14–16] designed a foil device extracting energy in non-sinusoidal motion and conducted numerical simulations on the power output, the extraction efficiency and the feasibility of this device. Xiao et al. [17,18] carried out an analysis of different non-sinusoidal pitching motions which are similar to trapezoidal ones, their research revealed that foil under non-sinusoidal motions like trapezoid motion has a higher power output and extraction efficiency at some *St* number. Ashraf [19] discussed the effect of different non-sinusoidal motions on the flow field around the foil. They found that the power coefficient of non-sinusoidal motions improved by 17% compared to sinusoidal motion.

Recently, research about the effect factors of foil extraction performance has been becoming more and more perfect and complete. However, most research focused on single foil and only a few of the researchers analyzed the extraction characteristics of foils under parallel configuration. According to our previous research [20], the flow field around two parallel foils will affect each other during the oscillation motions, which results in a better performance than that around the single foil. Therefore, it is necessary to further explore the influence of non-sinusoidal motion to the energy extraction performance of parallel foils.

In this paper, two oscillation motions are considered, which are the combined non-sinusoidal plunging and sinusoidal pitching motion, as well as the combined non-sinusoidal pitching and sinusoidal plunging motion. The numerical analysis of energy extraction characteristics is conducted. The rest of this paper is introduced as follows. Firstly, the computation model, the numerical method and the oscillation control equations of parallel foils are described. Then, the energy extraction characteristics of parallel foils under two different combined motions are analyzed in detail. Finally, the conclusions about the effect from non-sinusoidal motions are drawn.

2. Numerical Model and Method

2.1. Model of Parallel Foils

The parallel foils considered in this paper are two-dimensional NACA 0012 airfoils with the chord length c = 1 m. As shown in Figure 1, two foils are arranged next to each other along the vertical direction of the chord length, and the space between the two foils is δ. Parallel foils move in the combined plunging and pitching motion, the foil A and foil B (see Figure 1) are the starting positions of foil oscillation. As the oscillation starts, the foils move outwards during t/T = 0–0.5. The transient pitching angle $\alpha(t)$, plunging displacement $h(t)$, pitching amplitude θ_0 and plunging amplitude H_0 are shown in Figure 1. While the parallel foils move to their plunging limited positions, the foils start the reserve motions. The foils get closer and closer during t/T = 0.5–1, and finally, they get back to the starting position. An oscillation cycle of the foils has thus finished. The pitching axis of the foil is one-third chord length to the leading edge of the foil and δ is selected as 1.2 m throughout the whole numerical analysis.

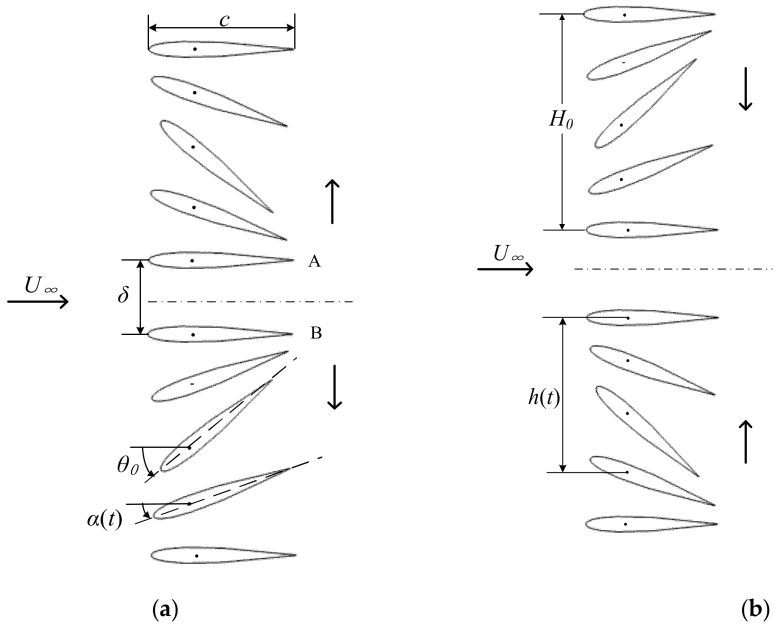

Figure 1. The structure and oscillation process of parallel foils: (**a**) t/T = 0–0.5; (**b**) t/T = 0.5–1.

2.2. Numerical Method

According to the finite volume method, the numerical simulations of the parallel foils oscillating in different non-sinusoidal motions are conducted by the commercial software Fluent 16.0 and the incompressible viscous flow field around foils is analyzed. The spatial term is discretized in the form of the second-order upwind type, while the transient term is discretized by the second-order-accurate backward implicit scheme [21]. All cases are investigated at Re = 1100, and the laminar model is selected to discuss the evolution law of the flow field around parallel foils.

2.3. Design of Computation Domain

In order to save computation resources and time while keeping a high simulation accuracy, the computation domain of the parallel foils is divided into several parts. The region close to the parallel foils is the inner zone, and the region outside the inner zone is the outer zone, as shown in Figure 2. Along the parallel foils' surface, the no-slip boundary condition is adopted. The interface between the inner and outer zone is set as the interface which connects the structured mesh and unstructured mesh. The velocity inlet is defined as U_∞ = 1 m/s and the pressure outlet is set. Based on the C programming language, the plunging and pitching motion characteristics in all simulations are controlled by the user-defined function (UDF) in Fluent. The dynamic mesh technique is applied to realize the reasonable transformation and reconstruction in the inner zone during the oscillation process, the quality of grids around the parallel foils is kept at a proper accuracy.

As displayed in Figure 3, large transformation due to the oscillation of foils occurs in the inner zone grid. Thus, the unstructured mesh is selected for the inner zone, which is denser and where it is easier to improve the grid quality. The structured mesh is adopted at the foil surface to ensure the computation accuracy of the boundary layer near the foil surface. For the outer zone, there is a much smaller transformation during oscillation, so the sparse structured mesh is used here to save the computation time. The mesh contains 7.5×10^4 cells, the height of the first cell in the boundary layer is set as $10^{-5}c$ to satisfy the computation accuracy.

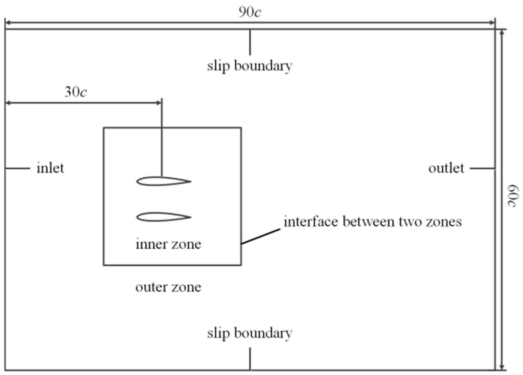

Figure 2. The computation domains arrangement.

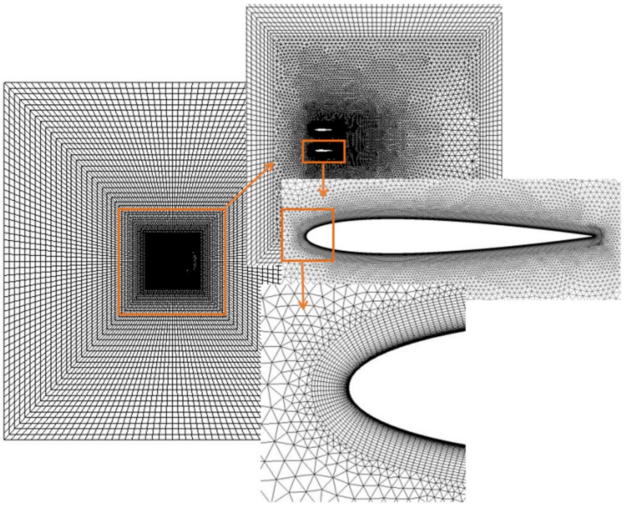

Figure 3. The mesh strategy.

2.4. Kinematics

The frequency of the parallel foils applied in this paper is the reduced frequency, which is the non-dimensional frequency. It is defined as follows:

$$k = \frac{2\pi f c}{U_\infty} \tag{1}$$

where f represents the frequency, c represents the chord length of foil, U_∞ represents the velocity of the free stream.

Based on the research of Xiao et al. [17], the power coefficient shows a similar trend under the different nominal angle of attack α_0. α_0 is set at 15° in this paper, the corresponding pitching amplitude θ_0 can be calculated as follows:

$$\theta_0 = \arctan\left(\frac{2\pi f H_0 c}{U_\infty}\right) + \alpha_0 \tag{2}$$

where H_0 is the dimensionless plunging amplitude and it is set at 1.

Our previous study focused on parallel foils with combined sinusoidal plunging and sinusoidal pitching motion [20]. To discuss the effect of non-sinusoidal motion, the energy extraction characteristics of parallel foils under the combined non-sinusoidal plunging and sinusoidal pitching motion, as well as the combined non-sinusoidal pitching and sinusoidal plunging motion, are both investigated. Sinusoidal pitching oscillation and sinusoidal plunging oscillation are defined as Equations (3) and (4):

$$\alpha(t) = \theta_0 \sin(2\pi f t + \beta) \tag{3}$$

$$h(t) = H_0 c \sin(2\pi f t + \phi + \beta) \tag{4}$$

where β for the upper foil is set at 180° and β for the lower foil is set at 0°. φ represents the phase difference between the plunging motion and pitching motion; φ is set as 90° [10].

The non-sinusoidal pitching motion is calculated based on the control parameter of pitching motion K_θ:

$$\alpha(t) = \begin{cases} \frac{\theta_0 \sin^{-1}[-K_\theta \sin(2\pi f t+\beta)]}{\sin^{-1}(-K_\theta)}, & -1 \le K_\theta < 0 \\ \theta_0 \sin(2\pi f t + \beta), & K_\theta = 0 \\ \frac{\theta_0 \tanh[K_\theta \sin(2\pi f t+\beta)]}{\tanh K_\theta}, & K_\theta > 0 \end{cases} \tag{5}$$

In a similar way, non-sinusoidal plunging motion is calculated based on the control parameter of plunging motion K_h:

$$h(t) = \begin{cases} \frac{H_0 c \sin^{-1}[-K_h \sin(2\pi f t+\phi+\beta)]}{\sin^{-1}(-K_h)}, & -1 \le K_h < 0 \\ H_0 c \sin(2\pi f t + \phi + \beta), & K_h = 0 \\ \frac{H_0 c \tanh[K_h \sin(2\pi f t+\phi+\beta)]}{\tanh K_h}, & K_h > 0 \end{cases} \tag{6}$$

In this paper, different non-sinusoidal plunging motions and non-sinusoidal pitching motions are considered, including the cases under $K_h = -1$, -0.5, 0, 1 and 2 as well as the cases under $K_\theta = -1$, -0.5, 0, 1 and 2. The curves of the five non-sinusoidal plunging motions and non-sinusoidal pitching motions at $k = 0.8$ are presented in Figure 4a,b, respectively.

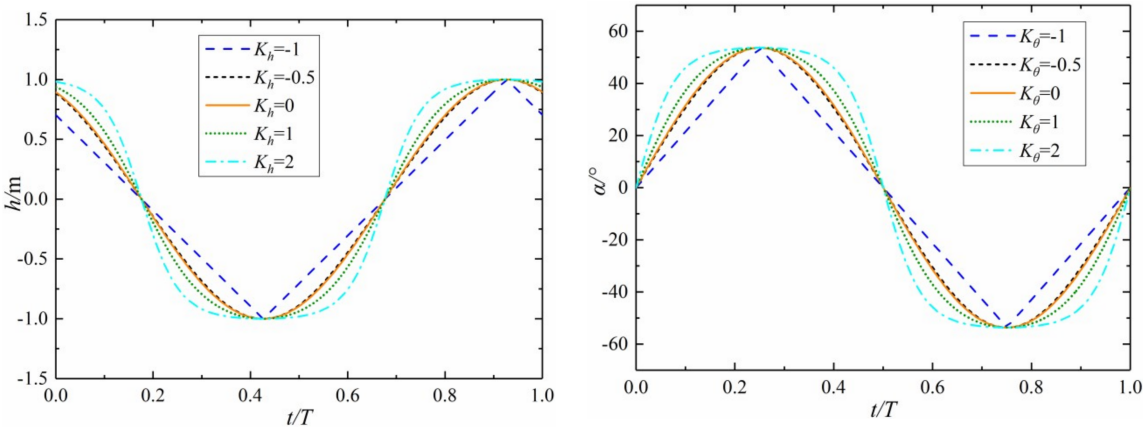

(**a**) (**b**)

Figure 4. The curves under the different non-sinusoidal motions at $k = 0.8$: (**a**) non-sinusoidal plunging motion; (**b**) non-sinusoidal pitching motion.

The energy extraction process of the foil over one cycle consists of two parts, the plunging oscillation and the pitching oscillation, the power output P is defined as follows:

$$P = F_y(t) V_y(t) + M(t)\omega(t) \tag{7}$$

where $F_y(t)$ is the lift force in the direction of the y-axis, $M(t)$ is the torque, $\omega(t)$ is the velocity of the pitching oscillation.

The transient power coefficient C_P can be computed by Equation (8):

$$C_P = \frac{P}{\frac{1}{2}\rho U_\infty^3 c} \tag{8}$$

The average power coefficient is composed by the pitching motion part and the plunging motion part, the definition is shown as follows:

$$C_{Pm} = C_{Phm} + C_{P\theta m} = \frac{1}{TU_\infty}\int_0^T \left[C_l(t)V_y(t) + C_m(t)\omega(t)\right]dt \tag{9}$$

The lift force coefficient C_l and the torque coefficient C_m are defined as Equations (10) and (11):

$$C_l = \frac{F_y}{\frac{1}{2}\rho U_\infty^2 c} \tag{10}$$

$$C_m = \frac{M}{\frac{1}{2}\rho U_\infty^2 c^2} \tag{11}$$

The extraction efficiency η is computed as the ratio of the extracted power to the total power of the free stream flow in the swept area, the definition is as Equation (12):

$$\eta = \frac{P_m}{\frac{1}{2}\rho U_\infty^3 A} = C_{Pm}\frac{c}{A} \tag{12}$$

where A represents the area of the foil's swept region, which is selected as $2H_0c$ [17].

2.5. Validation study

The grid independent and time-independent validation are conducted to ensure that the mesh strategy adopted and the time step set in the simulation have no influence on the analysis accuracy. As shown in Figure 5, three kinds of grids are selected, which are 5.2×10^4 cells, 7.5×10^4 cells and 1.12×10^5 cells, respectively. At the same time, three kinds of time steps are adopted, which are 600, 1200 and 2400 time steps in one oscillation cycle, respectively. The variations of the transient power coefficient C_P in a cycle are obtained. The difference between the three kinds of mesh strategies is small enough to ignore. Additionally, the results among the tested time steps show little difference. Thus, the mesh strategy with 7.5×10^4 cells and 1200-time steps per cycle are adopted in all numerical simulations.

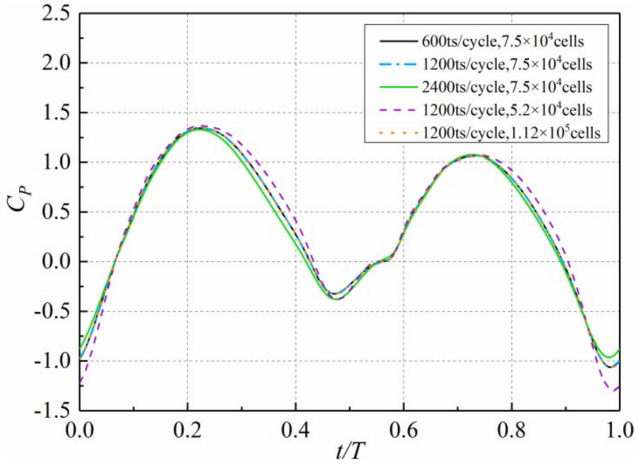

Figure 5. The variations of C_P under different mesh strategies and time steps.

3. Results and Discussions

3.1. Combined Non-Sinusoidal Plunging and Sinusoidal Pitching Motion

In this research, the energy extraction performance of parallel foils at combined non-sinusoidal plunging and sinusoidal pitching motion is investigated firstly. Five different plunging motions,

which are controlled by the non-sinusoidal plunging parameter K_h (K_h is set as -1, -0.5, 0, 1 and 2 respectively), are simulated. As shown in Figure 6, when K_h is -0.5, 0 and 1, the average power coefficient C_{Pm} ascends firstly and then decreases with the increasing k, showing a stable trend in general. At these three motions, all peak values of C_{Pm} appear at $k = 0.8$. Additionally, the maximal C_{Pm} is achieved when $K_h = -0.5$, which is 0.375. When $k < 1.0$, the best energy extraction performance of foil is observed at $K_h = -0.5$ under different k. Additionally, the optimal performance is gained at $K_h = 1$ when $k > 1.0$.

It is found from Figure 6 that C_{Pm} decreases obviously and becomes a negative value gradually with the increase in k when $K_h = -1$ and $K_h = 2$. This means these two oscillation motions are in the energy consumption situation and not the energy extraction situation in the range of frequency considered in this paper. It can be concluded from Figures 4 and 6 that, at the same frequency, the more the plunging motion is similar to the sinusoidal motion, the more the energy that can be extracted by parallel foils. At the same time, the extraction efficiency η shows a similar trend with the C_{Pm} curves at the non-sinusoidal plunging motion. When $k = 0.8$ and $K_h = -0.5$, the maximal extraction efficiency η is observed, which is 0.188.

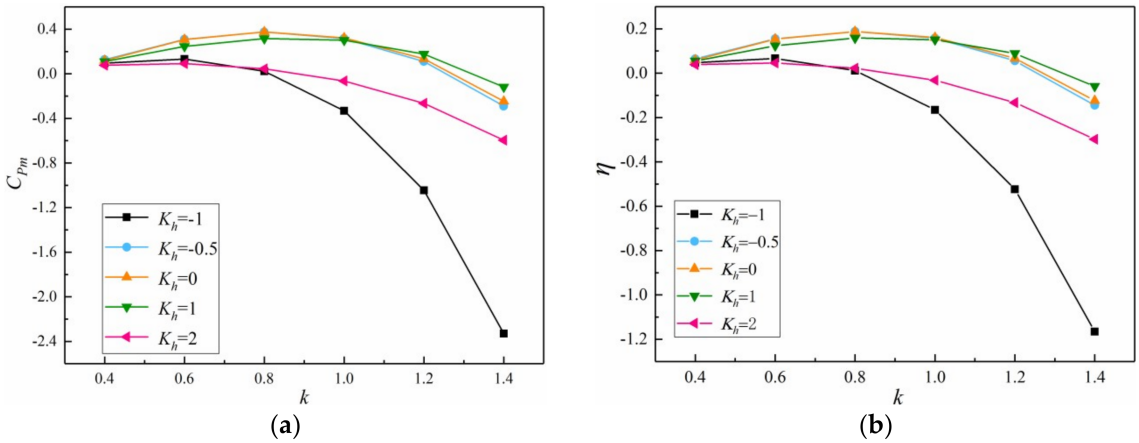

Figure 6. The C_{Pm} and η of parallel foils at different K_h: (**a**) C_{Pm} curves under different k; (**b**) η curves under different k.

Parallel foils in this paper oscillate as the combined plunging and pitching motion. Thus, to further investigate the effect factors and change law of energy extraction performance, the average power coefficient C_{Pm} is divided into the one caused by the plunging motion C_{Phm} and the one caused by pitching motion $C_{P\theta m}$. In general, the plunging motion is the process that extracting energy and the pitching motion is the process that consuming energy. However, as shown in Figure 7, when $K_h = -1$, the plunging motion converts the energy extraction situation into the energy consumption situation with increasing k. While the C_{Phm} increases gradually with the increasing k at the other four non-sinusoidal plunging motions. It indicates that the plunging motion with $K_h = -1$ is not appropriate to the energy extraction of the foil. For the pitching motion, they are all sinusoidal motion in different cases. In the figure, the little difference of $C_{P\theta m}$ at the same frequency is from the difference of the flow field caused by non-sinusoidal plunging motion. With the rise in k, $C_{P\theta m}$ declines obviously, which means the energy consumption increases. This is because the foil oscillates faster at high frequencies and the angular velocity of the adjusting process of the foil near the plunging limited position is higher, consuming more energy. In summary, the difference of C_{Pm} curves in Figure 6 is mainly from the different non-sinusoidal plunging motion.

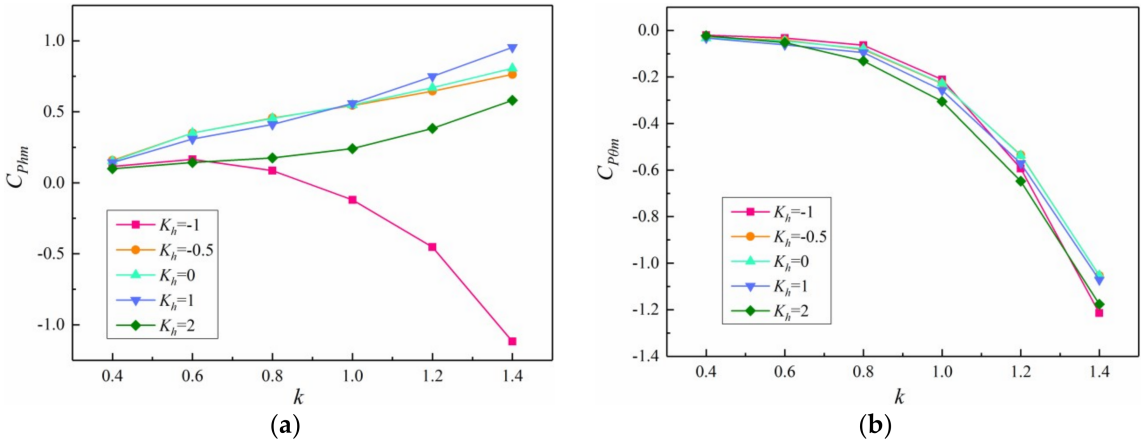

Figure 7. The C_{Phm} and $C_{P\theta m}$ of parallel foils at different K_h: (**a**) C_{Phm} curves under different k; (**b**) $C_{P\theta m}$ curves under different k.

The amount of energy extracted during the plunging oscillation process is related to the synchronicity between the lift coefficient C_l and the plunging velocity V_y. The C_l curves of the upper foil at $K_h = 0$ and $K_h = 2$ with $k = 0.8$ are shown in Figure 8. By comparing these two cases, it is concluded that the synchronicity of C_l and V_y is better at $K_h = 0$. While the synchronicity is not well at $K_h = 2$, even the totally opposite trend of C_l and V_y during $t/T = 0.17$–0.3 and $t/T = 0.67$–0.81 is observed. Although the peak value of C_l at $K_h = 2$ is obviously higher than that at $K_h = 0$, the C_{Pm} at $K_h = 2$ is relatively low because of the bad synchronicity of C_l and V_y. Thus, the energy extraction characteristics of foil are relatively poor when $K_h = 2$.

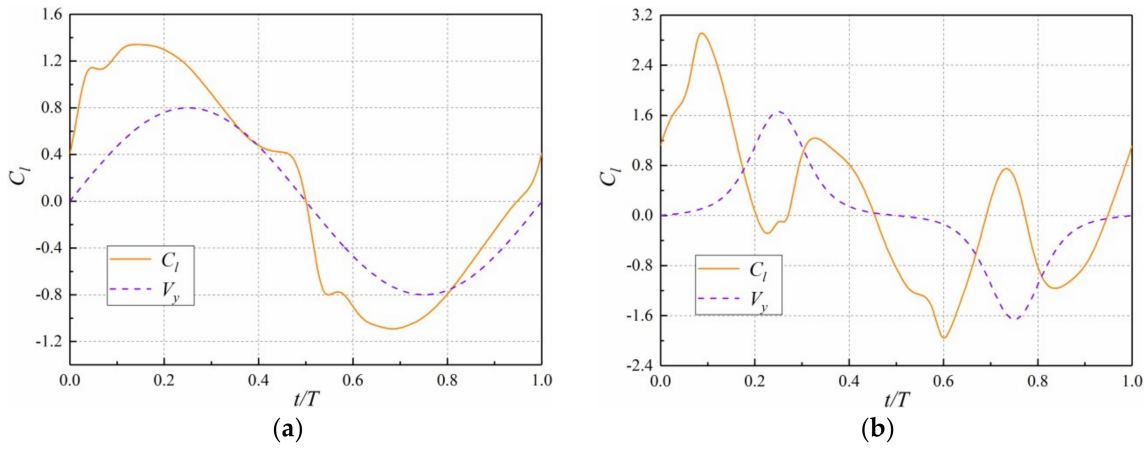

Figure 8. The C_l curves of the upper foil under different K_h at $k = 0.8$: (**a**) $K_h = 0$; (**b**) $K_h = 2$.

3.2. Combined Non-Sinusoidal Pitching and Sinusoidal Plunging Motion

The effects of the five different non-sinusoidal pitching motions on the extraction performance of parallel foils are considered. The motion of the foil is combined non-sinusoidal pitching and sinusoidal plunging motion. The non-sinusoidal pitching motion is controlled by the parameter K_θ. The energy extraction performance values at different K_θ and k are simulated, as shown in Figure 9. It can be found that the C_{Pm} at four kinds of motions ascends firstly and then decreases with increasing k, except the case at $K_\theta = -1$. The peak values of C_{Pm} at these four motions all appear at $k = 0.8$. This means $k = 0.8$ is the optimal frequency which could allow for the maximal power output in general. When $K_\theta = 2$, the maximal C_{Pm} is obtained, which is 0.623.

When the frequency is low, the effects of different oscillation motions on the energy extraction performance are less. With the increase in k, the influence from the non-sinusoidal pitching motion

on C_{Pm} increases. Foils go into the energy consumption situation earlier and faster in the case with $K_\theta = -1$ and $K_\theta = 2$ at high frequencies. The extraction efficiency η has the same trend with C_{Pm}. The optimal extraction efficiency η achieves 0.312 at $k = 0.8$ with $K_\theta = 2$.

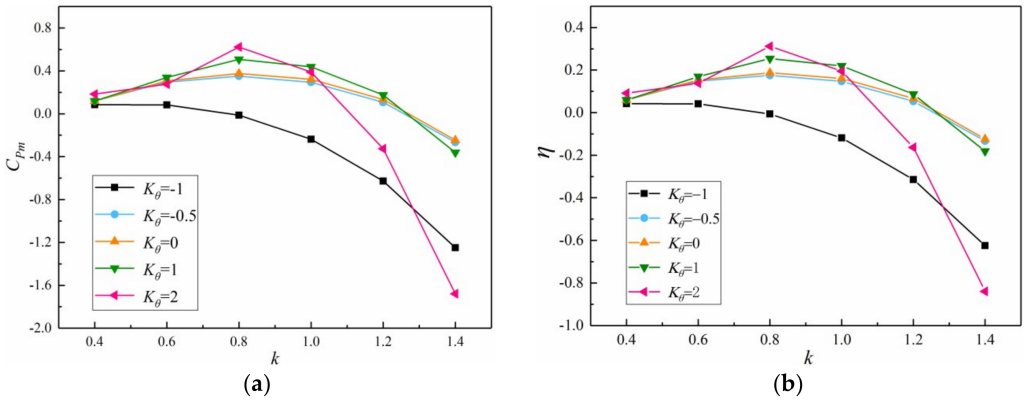

Figure 9. The C_{Pm} and η of parallel foils at different K_θ: (**a**) C_{Pm} curves under different k; (**b**) η curves under different k.

To investigate the influence of plunging motion and pitching motion on energy extraction, we separate C_{Pm} into the plunging part C_{Phm} and pitching part $C_{P\theta m}$, as shown in Figure 10. In the plunging oscillation process, the energy extracted by the plunging motion under four motions (except $K_\theta = -1$) ascends with the increasing k. This is due to the increasing frequency lifts the plunging velocity V_y of foil, more energy is extracted by plunging motion as a result.

When the frequency is relatively low, the different K_θ has little influence on the power consumption of the pitching motion. Some non-sinusoidal pitching motions obviously cause the energy consumption with the increase in k, like $K_\theta = 1$ and $K_\theta = 2$. This indicates that the more the non-sinusoidal pitching motion is similar to the square wave, the worse the extraction performance that is obtained. This is because the more the pitching motion is like a square wave, the higher the average pitching velocity in an oscillation cycle will be, causing higher energy consumption. That is the reason that causes the sharp decline of C_{Pm} at high frequencies in the case of $K_\theta = 2$ (see Figure 9).

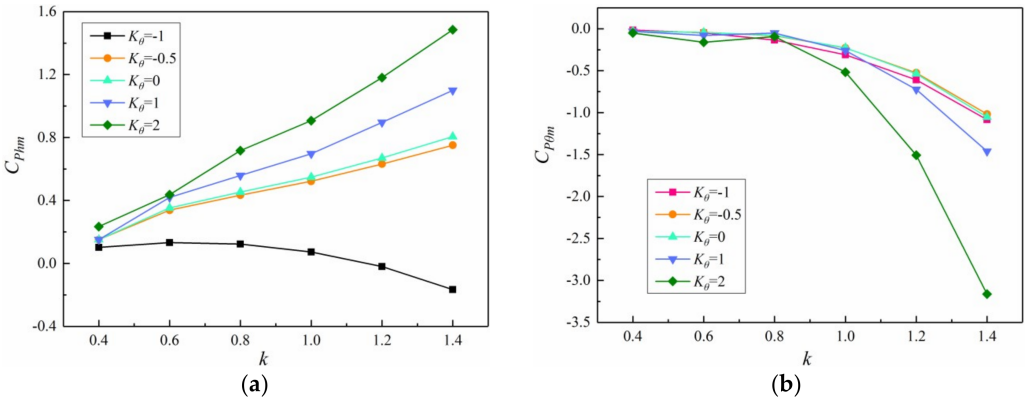

Figure 10. The C_{Phm} and $C_{P\theta m}$ of parallel foils at different K_θ: (**a**) C_{Phm} curves under different k; (**b**) $C_{P\theta m}$ curves under different k.

Figure 11 shows the C_l curves of the upper foil under two typical non-sinusoidal pitching motions $K_\theta = 1$ and $K_\theta = 2$ at $k = 0.8$. In these two cases, the plunging oscillation of the foil moves as with the same sinusoidal plunging motion. However, because of the effect from the non-sinusoidal pitching motion, the flow field around the foil is different, resulting in different forces in the y-direction. That is to say, the different pitching motions that cause different C_l values in the plunging motions are

the same. This explains the reason for different C_{Phm} at the same k in Figure 10. From Figure 11, it is observed that the synchronicity of C_l and V_y at these two motions is similar. When K_θ is 2, C_l fluctuates obviously near the plunging limited position, the peak value of C_l is higher. At the same time, C_l in an oscillation cycle at $K_\theta = 2$ is higher than that at $K_\theta = 1$ in general. Thus, from Figures 10 and 11, the case with $K_\theta = 2$ extracts more energy.

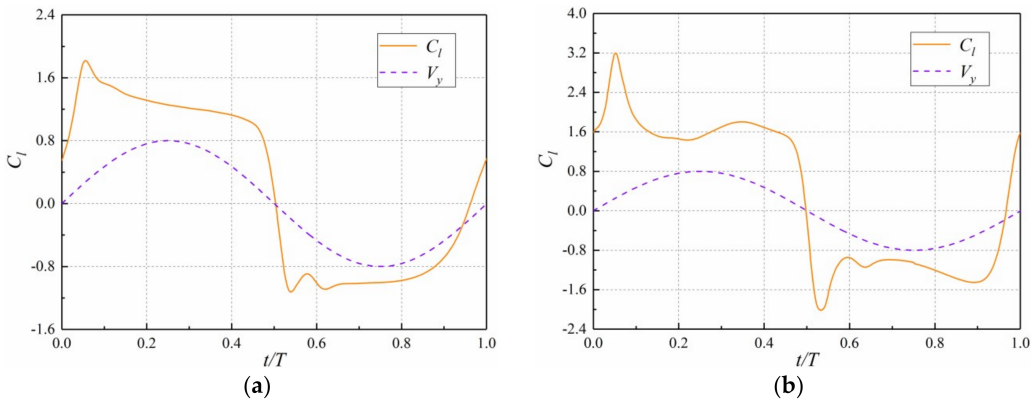

Figure 11. C_l curves of upper foil under different K_θ at $k = 0.8$: (**a**) $K_\theta = 1$; (**b**) $K_\theta = 2$.

To analyze the difference of the C_l curve at different non-sinusoidal pitching motions in Figure 11, we discuss the evolution of the vortex field around parallel foils in the cases of $K_\theta = 1$ and $K_\theta = 2$ during $t/T = 0$–0.5. Comparing the vortex field in Figure 12a,b, it is found that the vortex structures at $K_\theta = 2$ are bigger than those at $K_\theta = 1$ during every moment. The bigger low-pressure area is formed because of the bigger vortex structure, increasing the lift force. So C_l at $K_\theta = 2$ is higher than that at $K_\theta = 1$ in Figure 11. The C_l curve in Figure 11b has a significant fluctuation near $t/T = 0.05$, combining with Figure 12b. It is concluded that a big trailing edge vortex sheds at this time, causing a sharp change of C_l. Meanwhile, the leading edge vortex is formed earlier at $K_\theta = 2$.

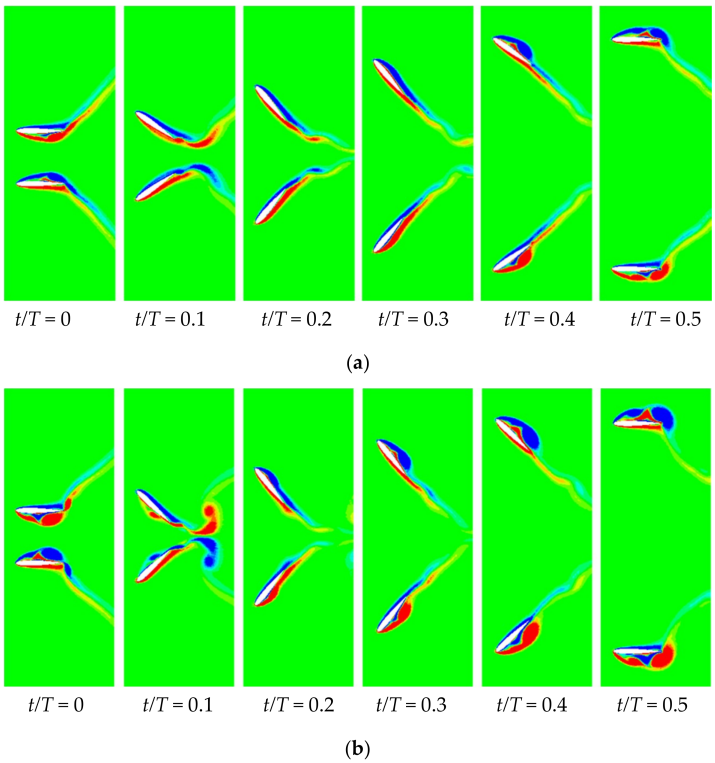

Figure 12. The vortex field during $t/T = 0$–0.5 under different K_θ at $k = 0.8$: (**a**) $K_\theta = 1$; (**b**) $K_\theta = 2$.

4. Conclusions

In this paper, we considered the effect of non-sinusoidal motion on the energy extraction performance of parallel foils. The energy extraction processes of two oscillation motions (the combined non-sinusoidal plunging and sinusoidal pitching motion, as well as the combined non-sinusoidal pitching and sinusoidal plunging motion) with Re = 1100 are simulated. Five non-sinusoidal motions are discussed and the optimal motion, the optimal frequency and the average power coefficient for these two combined oscillation motions are obtained. The contribution of plunging oscillation and pitching oscillation to energy extraction performance of foil is analyzed and the relationship between the lift force and the vortex structure is investigated.

The results show that both the non-sinusoidal plunging motion and the non-sinusoidal pitching motion have an obvious effect on the energy extraction characteristics of foil. When the foils oscillate as the combined non-sinusoidal plunging and sinusoidal pitching motion, the optimal extraction performance of foil appears when K_h is -0.5; the highest power output C_{Pm} and extraction efficiency η are 0.375 and 0.188, respectively. When $k < 1.0$, the combined motion with $K_h = -0.5$ shows a better extraction performance, while the better performance appears at the combined motion with $K_h = 1$ when $k > 1.0$. At the same k, the more the plunging motion approximates to the sinusoidal motion, the more energy is extracted by the parallel foils.

When the motion is the combined non-sinusoidal pitching and sinusoidal plunging, the peak values of C_{Pm} under four different motions (except $K_\theta = -1$) are gained at k = 0.8. This means that the optimal frequency which can gain the best extraction performance of foil in most motions is 0.8. The optimal C_{Pm} and η are achieved at $K_\theta = 2$, which are 0.623 and 0.312, respectively. At a high frequency, the effect of the non-sinusoidal pitching motion on the extraction performance is obvious. With the increase in k, the non-sinusoidal pitching motion at $K_\theta = 1$ and $K_\theta = 2$ cause a high consumption of energy. That is to say, the more the non-sinusoidal pitching motion is similar to the square wave, the worse extraction performance gained.

According to the vortex fields under different non-sinusoidal pitching motions, it was found that the vortex structure at $K_\theta = 2$ is much bigger than that at $K_\theta = 1$ at every moment. The lift force of foil is higher at $K_\theta = 2$, and the synchronicity between C_l and V_y at these two motions are similar. As a result, the oscillation process of the foils extracts more energy when K_θ is 2.

Author Contributions: Y.W. and Y.X. established the analysis method of the energy extraction performance of parallel foils; Y.W. performed the numerical investigation and obtained the conclusions. F.Z. established the computational model, discussed the results and wrote the paper.

Funding: This research was funded by the National Natural Science Foundation of China, project number is 11872294.

Conflicts of Interest: The authors declare no conflict of interest.

Nomenclature

A	foil's oscillation area, m^2
c	length of foil, m
C_l	lift coefficient
C_m	torque coefficient
C_P	power coefficient
f	frequency, Hz
F_y	aerodynamic lift force in y direction, N
$h(t)$	plunging motion
H_0	non-dimensional plunging amplitude
k	reduced frequency
K_h	control parameter of plunging motion
K_θ	control parameter of pitching motion
M	torque, N·m
P	power, W

Re	Reynolds number
St	Strouhal number
t	time, s
T	oscillation cycle, s
U_∞	free stream velocity, m·s^{-1}
$V_y(t)$	plunging velocity, m·s^{-1}
$\alpha(t)$	pitching motion
α_0	nominal angle of attack
δ	space between parallel foils, m
η	efficiency
θ_0	pitching amplitude, °
ρ	fluid density, kg·m^{-3}
φ	phase difference between plunging and pitching motion, °
ω	pitching velocity, rad·s^{-1}

Superscript

h	plunging motion
m	average value

References

1. McKinney, W.; DeLaurier, J. The wingmill: An oscillating-wing windmill. *J. Energy* **1981**, *5*, 109–115. [CrossRef]
2. Campobasso, M.S.; Drofelnik, J. Compressible Navier-Stokes analysis of an oscillating wing in a power-extraction regime using efficient low-speed preconditioning. *Comput. Fluids* **2012**, *67*, 26–40. [CrossRef]
3. Abiru, H.; Yoshitake, A. Study on a flapping wing hydroelectric power generation system. *J. Environ. Eng.* **2011**, *6*, 178–186. [CrossRef]
4. Shimizu, E.; Isogai, K.; Obayashi, S. Multiobjective design study of a flapping wing power generator. *J. Fluids Eng.* **2008**, *130*, 021104. [CrossRef]
5. Han, R.; Cherry, J.; Kallenberg, R. Modeling an oscillating water foil for hydro-kinetic power generator using COMSOL 3.5a. In Proceedings of the COMSOL Conference, Boston, MA, USA, 7–9 October 2010.
6. Jones, K.D.; Platzer, M.F. Numerical computation of flapping-wing propulsion and power extraction. In Proceedings of the 35th Aerospace Sciences Meeting and Exhibit, Reno, NV, USA, 6–9 January 1997.
7. Jones, K.D.; Lindsey, K.; Platzer, M.F. An investigation of the fluid-structure interaction in an oscillating-wing micro-hydropower generator. *Phys. Atom. Nucl.* **2003**, *65*, 325–328.
8. Kim, J.; Quang, L.T.; Hwan, K.J.; Sitorus, P.E.; Tambunan, I.H.; Kang, T. Experimental and numerical study of a dual configuration for a flapping tidal current generator. *Bioinspir. Biomim.* **2015**, *10*, 046015. [CrossRef] [PubMed]
9. Dumas, G.; Kinsey, T. Eulerian simulations of oscillating airfoils in power extraction regime. *Adv. Fluid Mech. VI* **2006**, 245–254. [CrossRef]
10. Kinsey, T.; Dumas, G. Parametric study of an oscillating airfoil in a power-extraction regime. *AIAA J.* **2008**, *46*, 1318–1330. [CrossRef]
11. Tuncer, I.H.; Kaya, M. Optimization of flapping airfoils for maximum thrust and propulsive efficiency. *AIAA J.* **2005**, *43*, 2329–2336. [CrossRef]
12. Bryant, M.; Shafer, M.W.; Garcia, E. Power and efficiency analysis of a flapping wing wind energy harvester. *Proc. SPIE* **2012**, *8341*, 83410E. [CrossRef]
13. Sitorus, P.E.; Le, T.Q.; Ko, J.H.; Truong, Q.T.; Tambunan, I.H.; Kang, T. Progress on development of a lab-scale flapping-type tidal energy harvesting system in KIOST. In Proceedings of the 2013 IEEE Conference on Clean Energy and Technology, Lankgkawi, Malaysia, 18–20 November 2013.

14. Platzer, M.F.; Sarigul-Klijn, N. A new oscillating-foil power generator for sailingship-based renewable energy generation. In Proceedings of the ASME 2010 4th International Conference on Energy Sustainability, Phoenix, AZ, USA, 17–22 May 2010.
15. Platzer, M.F.; Ashraf, M.A.; Young, J. Extracting power in jet streams: Pushing the performance of flapping-wing technology. In Proceedings of the 27th International Congress of the Aeronautical Sciences, Nice, France, 19–24 September 2010.
16. Platzer, M.F.; Young, J.; Lai, J.C.S. Flapping-wing technology: The potential for air vehicle propulsion and airborne power generation. In Proceedings of the 26th International Congress of the Aeronautical Sciences, Anchorge, AK, USA, 14–19 September 2008.
17. Xiao, Q.; Liao, W.; Yang, S. How motion trajectory affects the energy extraction performance of an oscillating foil. In Proceedings of the 48th AIAA Aerospace Sciences Meeting Including the New Horizons Forum and Aerospace Exposition, Orlando, FL, USA, 6 January 2010.
18. Xiao, Q.; Liao, W.; Yang, S.; Yan, P. How motion trajectory affects energy extraction performance of a biomimic energy generator with an oscillating foil. *Renew. Energy* **2012**, *37*, 61–75. [CrossRef]
19. Ashraf, M.A.; Young, J.; Lai, J.C.S.; Platzer, M.F. Numerical analysis of an oscillating-wing wind and hydropower generator. *AIAA J.* **2011**, *49*, 1374–1386. [CrossRef]
20. Wang, Y.L.; Jiang, W.; Xie, Y.H. Numerical investigation into the effects of motion parameters on energy extraction of the parallel foils. *J. Fluids Eng.* **2018**, *141*, 061104. [CrossRef]
21. Young, J.; Lai, J.C.S. Mechanisms influencing the efficiency of oscillating airfoil propulsion. *AIAA J.* **2007**, *45*, 1695–1702. [CrossRef]